

Back of the envelope calculations in friction stir welding – velocities, peak temperature, torque, and hardness

A. Arora, T. DebRoy and H. K. D. H. Bhadeshia*

Department of Materials Science and Engineering
The Pennsylvania State University, University Park, PA 16802, USA

*Department of Materials Science and Metallurgy
University of Cambridge, Cambridge CB2 3QZ, U.K.

Key words: friction stir welding; modeling; theory; velocity field; peak temperature; torque; hardness; aluminum alloys;

Abstract

Given the complexity and resource requirements of numerical models of friction stir welding (FSW), well-tested analytical models of materials flow, peak temperatures, torque, and weld properties are needed. Here an approximate analytical technique for the calculation of three-dimensional materials flow during FSW is proposed considering the motion of an incompressible fluid induced by a solid rotating disk. The accuracy of the calculations is examined for the welding of three alloys. For the estimation of peak temperatures, the accuracy of an existing dimensionless correlation is improved using a large volume of recently published data. The improved correlation is tested against experimental data for three aluminum alloys. It is shown that the torque can be calculated analytically from the yield stress using estimated peak temperatures. An approximate relation between the hardness of the thermomechanically affected zone and the chemical composition of the aluminum alloys is proposed.

Introduction

Recently developed numerical models of heat transfer, materials flow, torque and other parameters in friction stir welding (FSW) [1-53] have been tested against experimental data for the joining of aluminum alloys [2,4-13,52], steels [3,17,18,41,53] and titanium alloys.[49] These models have been applied for the solution of several problems. For example, the computed temperature and materials flow fields have been useful in understanding the heating and cooling rates, improvement of tool design [21,24,45,54-58] and in the estimation of torque and traverse force [16-18,21,24,49,54-55,59]. However, most of these numerical models require the solution

of the Navier Stokes equations and the energy equation together with the constitutive equations to obtain the viscosity of the plasticized materials. These calculations are complex and computationally intensive.

Sophisticated numerical models also exist for fusion welds, in parallel with simple but insightful methods, for example, those based on the Rosenthal equations [60] or carbon equivalents [61]; these analytical tools are used widely and form the basis for many practical judgments. A similar scenario does not exist for the much younger friction stir process. What is needed and not currently available, is a set of analytical methods to calculate important parameters such as the material flow fields, temperatures, torque and hardness of the thermomechanically affected zone (TMAZ). Here we propose several simplified methodologies to approximately estimate these important variables. Material flow during friction stir welding is driven mainly by the rotation of the tool shoulder. Therefore, we develop and test an approximate analytical technique for the calculation of this flow in three dimensions, based on viscous flow of an incompressible fluid induced by a solid rotating disk. The computed velocity fields for the welding of an aluminum alloy, a steel and a titanium alloy are compared with those obtained from a well tested and comprehensive numerical model. We also present an improved non-dimensional correlation to estimate the peak temperature, and an analytical method to estimate torque. The proposed correlation for the peak temperature is tested against experimental data for different weld pitch for three aluminum alloys. The computed torque values are tested against corresponding measurements for various tool rotational speeds. The hardness in the TMAZ has also been correlated with the chemical composition of aluminum alloys.

Velocity field

In order to develop an analytical solution for the three dimensional velocity field, the following assumptions are made. First, a relatively simple tool geometry with a straight cylindrical tool pin is considered. Second, the flow is assumed to result primarily from the rotation of the tool shoulder. Third, a known geometry of the flow domain based on many experiments is assumed. The material flow field is estimated by appropriately modifying an analytical solution for the steady state flow of a incompressible fluid between two solid disks, one rotating and the other stationary. [64] The three components of velocity, u , v , w in r , θ and z directions, respectively in cylindrical polar coordinates are given by:

$$u = r\omega F, v = r\omega G, \text{ and } w = d\omega H \quad (1)$$

where r is the radial distance, ω is the rotational velocity, d is the distance between the two disks, and the F , G and H are functions of z/d where z is the vertical distance under the rotating disk. The expressions F , G and H are explained in detail in the appendix. In order to adapt the above mentioned solution for FSW, it is necessary to define the material flow domain. The experimentally observed domain for material flow is shown schematically in Fig. 1. This zone has the shape of an inverted cone, truncated near the tip of the tool pin. The velocity field in the entire three dimensional flow region can be readily calculated using Eq. (1) if the velocity field at the tool shoulder is specified.

In order to specify the local velocities of plasticized materials at the tool shoulder – material interface, a condition of partial slip is considered. For a tool shoulder velocity of ωr , the velocity of material in contact with the tool shoulder surface is considered as $(1-\delta)\omega r$ where δ is the fraction of slip at the interface. The fraction of slip is considered to be function of the tool rotation speed and can be expressed as: [59]

$$\delta = 0.2 + 0.8 \times \left(1 - \exp\left(-\delta_0 \frac{\omega R_M}{\omega_0 R_S}\right) \right) \quad (2)$$

where δ_0 and ω_0 are constants, R_S is the radius of shoulder and R_M is the average of the pin and shoulder radius. The data used for calculations of velocities are presented in table 1. [17,49,59]

Peak Temperature

It has been recently shown that an existing dimensionless correlation of the following form can be useful for the estimation of non-dimensional peak temperature from the non-dimensional heat input: [62]

$$T^* = \alpha \log(Q^*) + \beta \quad (3)$$

where α and β are constants, and the non-dimensional peak temperature, T^* , is defined as: [62]

$$T^* = \frac{T_P - T_{in}}{T_S - T_{in}} \quad (4)$$

where T_P is the peak temperature, T_{in} is the initial temperature and T_S is the solidus temperature, Q^* is the non-dimensional heat input defined as: [62]

$$Q^* = \frac{\dot{\phi} A \dot{u} C_p \phi}{kU^2} \quad (5)$$

where σ_8 is the yield stress of the material at a temperature of $0.8T_s$, A is the cross sectional area of the tool shoulder, ω is the tool rotation velocity, C_p is the specific heat capacity of the workpiece material, k is the thermal conductivity of the workpiece, U is the traverse velocity and ϕ is the ratio in which heat generated at the shoulder workpiece interface is transported between the tool and the workpiece, and is defined as: [62]

$$\phi = \left[\frac{(k\tilde{n}\tilde{n}_p)_W}{(k\tilde{n}\tilde{n}_p)_T} \right]^{1/2} \quad (6)$$

where ρ is the density, and the subscripts W and T are used to describe the material properties of workpiece and the tool respectively. All the material properties are taken at a temperature average between the initial temperature and the solidus temperature.

Because of the availability of many recently reported values of peak temperatures in the literature, the coefficients α and β in Eq. (3) can now be based on a larger volume of reported peak-temperature data. As a result, the correlation is now more accurate than before.

Torque

The torque required during FSW determines the energy input to the workpiece and is also an important parameter in tool design. It is calculated from the shear stress at yielding, τ , which is given by: [16-18,59]

$$\tau = Y/\sqrt{3} \quad (7)$$

where Y is the yield stress at an average temperature on the tool shoulder workpiece interface. The average temperature, in turn, is calculated from the peak temperature. Previous research [16] has shown that the average temperature at the shoulder work piece interface is approximately 95% of the peak temperature (T_p). The value of T_p is estimated from the dimensionless correlation shown in Eq. (3). The total shear stress, τ_t , on the tool can be given as [18,59]

$$\tau_t = \left[(1 - \delta)\tau + \delta\mu_f P_N \right] \quad (8)$$

where δ is the fraction of slip computed from Eq. (2), μ_f is the friction coefficient and P_N is the axial pressure. The torque, T , can be computed from the total shear stress as follows: [18,59]

$$T = \oint_A \mathbf{r} \times (\tau_t dA) = \tau_t \int_0^{R_s} 2\pi r^2 dr = \frac{2\pi R_s^3 \tau_t}{3} \quad (9)$$

where r is the distance from tool axis, dA is the infinitesimal area on the shoulder workpiece contact surface and dr is the infinitesimal distance along the radial direction.

Hardness

For friction stir welding of steel welds, the hardness in the TMAZ has been correlated with the carbon equivalent, which is defined as [63]

$$CE = C + \frac{Mn + Si}{6} + \frac{Ni + Cu}{15} + \frac{Cr + Mo + V}{5} \quad (10)$$

where the element symbols refer to their concentrations in weight percent. However, friction stir welding is mostly used for the aluminum alloys and currently no such correlation for hardness is available for the welding of these alloys. The data available in the literature are used to develop a correlation between the hardness of the TMAZ material with the chemical composition of the alloy for the FSW of aluminum alloys.

Results and discussion

The first step in the proposed analytical calculation of three dimensional materials flow field in FSW is to estimate the material velocities at the interface between the shoulder and the workpiece. The maximum velocities at the top surface are $(1-\delta)\omega r$ where δ is the spatially dependent slip given by Eq. (2), ω is the rotational speed and r is the distance from the tool rotation axis. Once the velocities at the shoulder-workpiece interface are known, the velocity field in the entire flow domain is given by Eq. (1). For aluminum alloy AA2524 containing 4.3Cu, 1.4Mg, 0.58Mn wt% and small quantities of Si, Fe and Zn, the computed velocity fields in different horizontal planes parallel to the tool shoulder surface are compared with those in the same planes computed by three dimensional heat transfer and visco-plastic flow model in Fig. 2. A fair agreement in the flow pattern is observed between the numerically and analytically computed results in Fig. (2), The material velocity is maximum at $z = 0$ (the tool shoulder workpiece interface) and decreases as the distance from the tool shoulder increases. The analytically computed velocities at various locations are quantitatively compared with the correspondingly numerically computed results as explained below.

Fig. 3 shows the velocities, computed from both analytical solution and 3D comprehensive numerical visco-plastic flow and heat transfer model, as a function of the vertical

distance below the tool shoulder. The velocity u' in this figure is the square root of the sum of the three velocity components squared. The velocities in the three plots for the welding of an aluminum alloy, a steel and a titanium alloy are made non-dimensional by dividing with the maximum velocity (u^*). These velocities are plotted against the non-dimensional vertical distance from the shoulder defined by z/d , where d is the pin length. The velocities in the three cases are maximum at the tool workpiece interface where z/d is zero and decrease as the distance from the tool shoulder increases. The results from the analytical solution are in fair agreement with the 3D heat transfer and visco-plastic flow model for FSW of AA2524, Ti-6Al-4V and 304L SS alloys. In each case, at horizontal planes near the mid-height of the tool pin, the analytical solutions predict about 10 to 17% higher velocities than the corresponding numerically computed velocities. This discrepancy can be attributed, at least in part, due to the difference between the computational and the physical flow domains. The actual wall of the flow domain is often closer than the wall of the inverted truncated cone assumed in the calculations. Other possible sources of discrepancy include the effects of the presence of the tool pin and the welding velocity which are not considered directly in the analytical model.

The non-dimensional temperature, defined by Eq. (3), is plotted as a function of the non-dimensional heat input using various experimental and numerically computed results obtained from the literature. The coefficients α and β for the Eq. 3 are recalculated from experimental results including recently published experimental results. The following correlation is proposed to estimate the non-dimensional peak temperature from the non-dimensional heat input on the basis of the results shown in Fig. 4:

$$T^* = 0.151 \log_{10}(Q^*) + 0.097 \quad (11)$$

This relationship is valid in the range of Q^* between 4×10^2 and 3.7×10^5 . It should be noted that the correlation has a standard deviation of 0.01 which is an improvement over the previous results [62] because of the inclusion of many recently published results. Furthermore, equation (11) is now valid for a larger range of Q^* .

The accuracy of the correlation developed in Eq. (11) is evaluated by estimating the peak temperatures at different weld pitch values and comparing the estimated results with corresponding experimental observations. Fig. 5(a) shows the experimentally measured peak temperatures [66] for various welding pitch values for aluminum 2024, 5083 and 7075 alloys. The estimated values of peak temperature for the same alloys are shown in Fig. 5(b). The data

used for the computation is shown in table 2. Since the tool dimensions and welding speed are not provided by Nakata et al. [66], commonly used tool dimensions (25 mm shoulder diameter and 6 mm pin diameter) and 400 mm/min welding velocity have been used for the calculations. It can be observed that the slopes of the estimated peak temperatures for the three alloys are similar to the slopes for experimental results. In both the experimental [66] and the analytical results, the peak temperature is highest for AA5083 and lowest for AA7075 for a specific weld pitch. The computed peak temperatures for various cases are 3 to 9% different from the corresponding experimentally determined values.

The experimentally measured values of the torque for friction stir welding of AA2524 and Ti-6Al-4V alloys are compared with the estimated torque from Eq. (9). Fig. 6 compares the analytically estimated and the experimentally measured torque values for FSW at various tool rotational speeds. It is observed that the torque required decreases with increase in the tool rotational speed for the FSW of both AA2524 and Ti-6Al-4V alloys. The material becomes softer with increase in temperature as the tool rotational speed increases, making it easier for the tool to rotate the material around. The analytically estimated values of the torque are in close agreement with the experimentally observed values of torque for both AA2524 and Ti-6Al-4V alloys. The torque values for Ti-6Al-4V are higher compared to AA2524 as the former is a harder material.

The hardness for friction stir welded steels was correlated to the carbon equivalent (*CE*) in Eq. 10. [63] Fig. 7 shows the hardness of various steels as a function of their carbon equivalent. The compositions of these steels are available in the literature. [63] In a similar manner, the hardness of the friction stir welded aluminum alloys has also been analyzed as a function of their chemical composition. Experimentally measured Vickers hardness values for various aluminum alloys are listed in table 3. Constrained multivariate regression analysis is used to develop a correlation between the composition of an aluminum alloy and the hardness values in TMAZ of the friction stir welded aluminum alloys. The following correlation is obtained:

$$HV = 17.15 + 35.88 \times Si + 30.38 \times Fe + 14.26 \times Cu + 13.01 \times Mn + 14.49 \times Mg + 11.90 \times Cr + 4.34 \times Zn + 37.40 \times Ti \quad (12)$$

where the element symbols refer to their concentration in weight percent. The correlation was obtained for the following range of alloying elements: Si 0.1-0.52 wt%, Fe 0.1-0.45 wt%, Cu 0.01-4.29 wt%, Mn 0-0.7 wt%, Mg 0.02-4.62 wt%, Ti 0-0.25 wt%, Zn 0-6.2 wt% and Cr 0-0.1

wt%. Fig. 8 shows a comparison of the hardness values estimated using Eq. (12) with the experimentally measured Vickers hardness values for various aluminum alloys. [67-76] It can be seen that the estimated TMAZ hardness values obtained from Eq. (12) agree well with the experimentally measured TMAZ hardness values for FSW of several aluminum alloys.

A computer program for the analytical calculation of velocity fields, and spreadsheets for the calculations of peak temperature, torque and the TMAZ hardness in FSW are available for download from <http://www.matse.psu.edu/modeling>.

Summary and conclusions

Analytical models of materials flow, peak temperatures, torque, and hardness for friction stir welding (FSW) are proposed and tested. The analytical solution for the calculation of three dimensional materials flow velocities during FSW is adapted from the analytical solution of the viscous flow of an incompressible fluid induced by a solid rotating disk. It is shown that such calculations are straightforward and fairly accurate for the FSW of an aluminum alloy, a steel and a titanium alloy. An existing correlation for the estimation of peak temperature is improved using a large volume of recently published data. The improved correlation for peak temperature is tested against experimental peak temperatures for different welding pitch for three aluminum alloys. The torque required for FSW at various tool rotational speeds were computed analytically from the yield stress of the materials using the peak temperature estimation proposed in this paper. Approximate correlations between the hardness of the TMAZ and the chemical composition of various aluminum alloys are suggested based on the data available in the literature. The methodologies proposed and tested in this paper allow calculation of important parameters in FSW without time-consuming and complex calculations.

Appendix A : Analytical calculation of the flow field

Here an analytical solution for the steady state flow of an incompressible fluid between two parallel discs, one rotating with a constant angular speed and the other at rest, is described. The two discs are separated by a distance d , the rotating disk is at $z = 0$ and the stationary disc is at $z = d$. In the cylindrical coordinate system, the continuity and momentum equations are as follows: [64]

$$2F + H' = 0 \quad (\text{A.1})$$

$$R(F^2 - G^2 + F' H) = F'' + \acute{a}_c R(F'^2 - 2FF' - G'^2) - 2P_1 \quad (\text{A.2})$$

$$R(2FG + G' H) = G'' + 2\acute{a}_c R(F' G' - FG'') \quad (\text{A.3})$$

$$R(HH') = P' + H'' + \acute{a}_c R(8H' H'' - 4FF') + \frac{r^2}{d^2} [2\acute{a}_c R(G' G'' + F' F'') - P_1'] \quad (\text{A.4})$$

where R is Reynolds number $R = \frac{\dot{\omega} d^2}{\delta_v}$, and $\acute{a}_c = \frac{\delta_c}{d^2}$, with ν_v and ν_c as the kinematic coefficients of viscosity and cross-viscosity. [64] The function F , G and H are functions of a dimensionless parameter η and define the velocity components u , v , w in the r , θ , z direction respectively. The velocity components are taken in the following form for the above mentioned simplification: [64]

$$u = r\omega F(\eta), \quad v = r\omega G(\eta), \quad w = d\omega H(\eta) \quad \text{for } \eta = z/d \quad (\text{A.5})$$

where ω is the angular velocity of the rotating disc. By solving (A.2) and (A.4) we can obtain [64]

$$R(F^2 - G^2 + F' H) = F'' - \acute{a}_c R(F'^2 + 2FF'' + 3G'^2) - 2\ddot{e} \quad (\text{A.6})$$

where λ is an integration constant. For small values of R , a regular perturbation scheme for the Eq. (A.1), (A.3), and (A.6) can be developed by expanding F , G , H , λ in powers of R : [64]

$$\begin{aligned} F &= f_0 + f_1 R + f_2 R^2 + f_3 R^3 + \dots \\ G &= g_0 + g_1 R + g_2 R^2 + g_3 R^3 + \dots \\ H &= h_0 + h_1 R + h_2 R^2 + h_3 R^3 + \dots \\ \lambda &= \lambda_0 + \lambda_1 R + \lambda_2 R^2 + \lambda_3 R^3 + \dots \end{aligned} \quad (\text{A.7})$$

Substituting F , G , H and λ from (A.7) in (A.3), (A.6) and equating the coefficients of different powers of R on both sides of these equations reduces the boundary conditions to [64]

$$f_0 = 0, \quad g_0 = 1, \quad h_0 = 0 \quad \text{at} \quad \eta = 0,$$

$$f_0 = 0, \quad g_0 = 0, \quad h_0 = 0 \quad \text{at} \quad \eta = 1, \quad (\text{A.8})$$

and for $n = 1, 2, 3 \dots$ [64]

$$\begin{aligned} f_n &= 0, & g_n &= 0, & h_n &= 0 & \text{at} & \eta = 0, \\ f_n &= 0, & g_n &= 0, & h_n &= 0 & \text{at} & \eta = 1, \end{aligned} \quad (\text{A.9})$$

Solution for f_n, g_n, h_n and λ_n for $n = 1, 2, 3 \dots$ can be found and F, G and H can be expressed in terms of f_n, g_n, h_n, λ_n and R as follows: [64]

$$\begin{aligned} F &= R \left(\frac{1}{10} \eta - \frac{7}{20} \eta^2 + \frac{1}{3} \eta^3 - \frac{1}{12} \eta^4 \right) + \\ &\left[\begin{aligned} &-0.000115\eta + 0.000219\eta^2 + 0.000714\eta^3 - 0.000714\eta^4 - 0.002167\eta^5 \\ &+ 0.003639\eta^6 - 0.002619\eta^7 + 0.001262\eta^8 - 0.000243\eta^9 + 0.000024\eta^{10} \\ &+ \alpha_c \left(\begin{aligned} &-0.004161\eta + 0.021661\eta^2 - 0.046667\eta^3 + 0.065\eta^4 \\ &- 0.063333\eta^5 + 0.037222\eta^6 - 0.011111\eta^7 + 0.001389\eta^8 \end{aligned} \right) \\ &+ \alpha_c^2 \left(\begin{aligned} &0.018095\eta - 0.001428\eta^2 - 0.2\eta^3 + 0.35\eta^4 - 0.2\eta^5 + 0.033333\eta^6 \end{aligned} \right) \end{aligned} \right] \quad (\text{A.10}) \end{aligned}$$

$$G = (1 - \eta) + R^2 \left[\begin{aligned} &-\frac{3}{700} \eta + \frac{1}{30} \eta^3 - \frac{1}{15} \eta^4 + \frac{17}{300} \eta^5 - \frac{1}{45} \eta^6 + \frac{1}{315} \eta^7 \\ &+ \alpha_c \left(\begin{aligned} &\frac{1}{10} \eta^2 - \frac{7}{30} \eta^3 + \frac{1}{6} \eta^4 - \frac{1}{30} \eta^5 \end{aligned} \right) \end{aligned} \right] \quad (\text{A.11})$$

$$\begin{aligned} F &= R \left(-\frac{1}{10} \eta^2 + \frac{7}{30} \eta^3 - \frac{1}{6} \eta^4 - \frac{1}{30} \eta^5 \right) + \\ &\left[\begin{aligned} &-0.000105\eta^2 - 0.000146\eta^3 - 0.000357\eta^4 + 0.000286\eta^5 + 0.000722\eta^6 \\ &- 0.00103\eta^7 + 0.000655\eta^8 - 0.00028\eta^9 + 0.000049\eta^{10} - 0.000004\eta^{11} \\ &+ \alpha_c \left(\begin{aligned} &0.004162\eta^2 - 0.014441\eta^3 + 0.023334\eta^4 - 0.026\eta^5 \\ &+ 0.021111\eta^6 - 0.010635\eta^7 + 0.002778\eta^8 - 0.000309\eta^9 \end{aligned} \right) \\ &+ \alpha_c^2 \left(\begin{aligned} &-0.018095\eta^2 + 0.000952\eta^3 + 0.1\eta^4 - 0.14\eta^5 + 0.066667\eta^6 - 0.009524\eta^7 \end{aligned} \right) \end{aligned} \right] \quad (\text{A.12}) \end{aligned}$$

In cartesian coordinate system r and η can be computed as follows:

$$r = \left(x^2 + y^2 \right)^{1/2}, \quad \zeta = z/d \quad (\text{A.13})$$

The computed velocity components are in cylindrical coordinates, and can be converted to the Cartesian coordinate system as follows:

$$u_{cart} = u_{cyl} \cos(\theta) - v_{cyl} \sin(\theta) \quad (\text{A.14})$$

$$v_{cart} = u_{cyl} \sin(\theta) + v_{cyl} \cos(\theta) \quad \text{where} \quad \tan(\theta) = \frac{y}{x} \quad (\text{A.15})$$

$$w_{cart} = w_{cyl} \quad (\text{A.16})$$

References:

1. McClure JC, Tang W, Murr LE, Guo X, Feng Z, Gould JE. A thermal model for friction stir welding. In: Vitek JM, David SA, Johnson JA, Smartt HB, DebRoy T (Eds.). Trends in welding research. Ohio, USA: ASM International; 1998. 590–5.
2. Russell MJ, Shercliff H. Analytical modelling of friction stir welding. In: Russell MJ, Shercliff R (Eds.). INALCO'98: 7th international conference on joints in aluminium. Cambridge, UK: TWI; 1999. 197–207.
3. Feng Z, Gould JE, Lienert TJ. A heat flow model for friction stir welding of steel. In: Bieler TR (Eds.). Hot deformation of aluminium alloys. Warrendale, PA, USA: TMS–AIME; 1998. 149–58.
4. Song M, Kovacevic R. Int J Mach Tools Manuf 2003;43:605.
5. Song M, Kovacevic R. J Eng Manuf 2003;217:73.
6. Song M, Kovacevic R. J Eng Manuf 2004;218:17.
7. Zhang HW, Zhang Z, Chen JT. Acta Metall Sin 2005;41:853.
8. Zhang HW, Zhang Z, Chen JT. Mater Sci Eng A 2005;403:340.
9. Chen CM, Kovacevic R. Int J Mach Tools Manuf 2003;43:1319.
10. Schmidt H, Hattel J, Wert J. Modell Simul Mater Sci Eng 2004;12:143.
11. Schmidt H, Hattel J. Int J Offshore Polar Eng 2004;14:296.
12. Schmidt H, Hattel J. Sci Technol Weld Join 2005;10:176.
13. Schmidt H, Hattel J. Modell Simul Mater Sci Eng 2005;13:77.
14. Khandkar MZH, Khan JA. J Mater Process Manuf Sci 2001;10:91.
15. Khandkar MZH, Khan JA, Reynolds AP. Sci Technol Weld Join 2003;8:165.
16. Nandan R, Roy GG, DebRoy T. Metall Mater Trans A 2006;37:1247.
17. Nandan R, Roy GG, Lienert TJ, DebRoy T. Sci Technol Weld Join 2006;11:526.
18. Nandan R, Roy GG, Lienert TJ, DebRoy T. Acta Mater 2007;55:883.
19. Simar A, Lecomte-Beckers J, Pardoën T, de Meester B. Sci Technol Weld Join 2006;11:170.
20. Colegrove PA, Shercliff HR. J Mater Process Technol 2005;169:320.
21. Colegrove PA, Shercliff HR. Sci Technol Weld Join 2004;9:345.
22. Bastier A, Maitournam MH, van Dang K, Roger F. Sci Technol Weld Join 2006;11:278.
23. Su P, Gerlich A, North TH, Bendzsak GJ. Sci Technol Weld Join 2006;11(2):163.
24. Colegrove PA, Shercliff HR. Sci Technol Weld Join 2004;9:352.
25. Lienert Jr TJ, Stellwag WL, Grimmatt BB, Warke RW. Weld J Res Suppl 2003;82:1s.
26. Xu S, Deng X, Reynolds AP, Seidel TU. Sci Technol Weld Join 2001;6:191.
27. Deng Z, Lovell MR, Tagavi KA. Manuf Sci Eng 2001;123:647.
28. Kong HS, Ashby MF. MRS Bull 1991;16:41.
29. Khan JA, Xu L, Chao YJ. Sci Technol Weld Join 1999;4:201.
30. Nandan R, Prabu B, De A, DebRoy T. Weld J 2007;86(10):313s.
31. De A, DebRoy T. Weld J 2005;84:101s.
32. De A, DebRoy T. J Phys D: Appl Phys 2006;37(1):140.
33. Kumar A, Zhang W, DebRoy T. J Phys D: Appl Phys 2005;38:119.
34. Kumar A, DebRoy T. Int J Heat Mass Transfer 2004;47(26):5793.
35. Zienkiewicz OC, Cormeau IC. Arch Mech 1972;24:872.
36. Sellars CM, McTegart WJ. Acta Metall 1966;14:1136.
37. Sheppard T, Wright DS. Met Technol 1979;6:215.
38. Wright DS, Sheppard T. Met Technol 1979;6:224.

39. Zener C, Hollomon JH. *J Appl Phys* 1944;15:22.
40. Sheppard T, Jackson A. *Mater Sci Technol* 1997;13:203.
41. Bruschi S, Poggio S, Quadrini F, Tata ME. *Mater Lett* 2004;58:3622.
42. Ulysse P. *J Mach Tools Manuf* 2002;42:1549.
43. Dong P, Lu F, Hong JK, Cao Z. *Sci Technol Weld Join* 2001;6:281.
44. Heurtier P, Jones MJ, Desrayaud C, Driver JH, Montheillet F, Allehaux D. *J Mater Process Technol* 2006;171:348.
45. Buffa G, Hua J, Shivpuri R, Fratini L. *Mater Sci Eng A* 2006;419:381.
46. Askari A, Silling S, London B, Mahoney M. *J Met* 2004;56:245.
47. Bell RL. An isotropic material remap scheme for Eulerian codes. In: 2nd International Conference on Cybernetics and Information Technologies, Systems and Applications (CITSA), 2005.
48. Boyce DE, Dawson PR, Sidle B, Gnäupel-Herold T. *Comput Mater Sci* 2006;38:158.
49. Nandan R, Lienert TJ, DebRoy T. *Int J Mater Res* 2008;99:434.
50. Bhadeshia HKDH. *Mater Sci Technol* 2008;24:128.
51. Seidel TU, Reynolds AP. *Sci Technol Weld Join* 2003;8:175.
52. Arora A, Zhang Z, De A, DebRoy T. *Scr Mater* 2009;61:863.
53. Bhadeshia HKDH, DebRoy T. *Sci Technol Weld Join* 2009;14:193.
54. Thomas WM, Johnson KI, Wiesner CS. *Adv Eng Mater* 2003;5:485.
55. Thomas WM. *Mater Sci Forum* 2003;426–432:229.
56. Thomas WM, Staines DG, Johnsonand KI, Evans P. *Adv Eng Mater* 2003;5:273.
57. Zhao YH, Lin SB, Qu F, Wu L. *Mater Sci Technol* 2006;22:45.
58. Mandal A, Roy P. *J Mater Process Technol* 2006;180:167.
59. Arora A, Nandan R, Reynolds AP, DebRoy T. *Scr Mater* 2009;60:13.
60. Rosenthal D. *Weld. J.* 1941;20(5):220s.
61. Suzuki H. Carbon equivalent and maximum hardness, IIW Document IX-1279-83, 1983.
62. Roy GG, Nandan R, DebRoy T. *Sci Technol Weld Join* 2006;11:606.
63. Nandan R, DebRoy T, Bhadeshia HKDH. *Prog Mater Sci* 2008;53(6):980.
64. Srivastava AC. *Q J Mech Appl Math* 1961;14(3):353
65. Lawrjaniec D, Abisror A, Decker C, Koçak M, Dos Santos J. *Mater. Sci. Forum* 2003;426-432:2993.
66. Nakata K, Kim YG, Ushio M, Hasimoto T, Jyogan S. *ISIJ Int.* 2000;40 (suppl.):S15.
67. Sato YS, Urata M, Kokawa H. *Metall Mater Trans A* 2002;33:625.
68. Sato YS, Kokawa H, Enomoto M, Jogan S. *Metall Mater Trans A* 1999;30:2429.
69. Reynolds AP, Tang W, Khandkar Z, Khan JA, Lindner K. *Sci Technol Weld Join* 2005;10:190.
70. Jata KV, Sankaran KK, Ruschau JJ. *Metall Mater Trans A* 2000;31:2181.
71. Liu HJ, Fujii H, Maedaa M, Nogi K. *J Mater Process Technol* 2003;142:692.
72. Sato YS., Urata M, Kokawa H, Ikeda K. *Mater Sci Eng A* 2003;354:298.
73. Adamowski J, Szkodo M. *J Achiev Mater Manuf Eng* 2007;20(1-2):403.
74. Boz M, Kurt A. *Mater Des* 2004;25(4):343.
75. Capelari1 TV, Mazzaferro JAE. *Soldag Insp (Impr.)* 2009;14(3):215.
76. Moreira PMGP, de Oliveira FMF, de Castro PMST. Mechanical characterization of friction stir welded aluminium alloy 6063-T6. 10th Portuguese conference on fracture 2006.

List of figures

Fig. 1 Schematic diagram showing the domain for velocity field calculation. An approximate thermomechanically affected zone (TMAZ) geometry is shown by cross hatched region in the figure.

Fig. 2 The computed velocity fields in various horizontal planes for the FSW of AA2524. (a) results from a well tested numerical heat transfer and visco plastic flow code, and (b) from the proposed analytical solution.

Fig. 3 The analytically computed velocities relative to the maximum velocity as a function of the dimensionless distance from the tool shoulder. (a) AA2524 (b) Ti-6Al-4V, (c) 304L SS. u' is the square root of sum of the three velocity components squared and u^* is the maximum velocity.

Fig. 4 Linear relationship between dimensionless temperature and log of dimensionless heat input.

Fig. 3 Peak temperature against weld pitch for friction stir welding of various aluminum alloys. (a) Experimentally measured peak temperature [66] (b) Peak temperature from the proposed correlation.

Fig. 4 Estimated and experimental torque values for FSW of (a) AA2524 and (b) Ti-6Al-4V alloy. The data used for the calculations are available in table 1.

Fig. 7 The Vickers hardness of the TMAZ as a function of the IIW carbon equivalent of the steel. [61]

Fig. 5 A comparison of the experimentally measured Vickers hardness of TMAZ during FSW of various aluminum alloys with that estimated from alloy composition. [67-76]

Table 1 Material properties and welding process parameters used in the velocity and torque estimation

| Alloy | AA2524 | 304L SS | Ti-6Al-4V |
|----------------------------------------------|------------------------------------|------------------------|--------------------------|
| Shoulder radius, R_S | 10.15 mm | 9.5 mm | 12.5 mm |
| Pin radius, R_P | 3.55 mm | 3 mm | 5 mm |
| Pin length | 6.2 mm | 6.4 mm | 9.9 mm |
| Rotating velocity, ω | 31.42 rad/s | 47.12 rad/s | 20.94 rad/s |
| Density, ρ | 2700 kg/m ³ | 7800 kg/m ³ | 4420 kg/m ³ |
| Axial pressure, P_N | 130.7 MPa | 130.7 MPa | 37.75 MPa |
| Constant for slip, δ_0 | 3.0 | 2.0 | 2.5 |
| Yield Strength, Y (Temperature, T in K) | $0.0062xT^2 - 7.61xT + 2371.5$ MPa | - | $-0.1406xT + 271.83$ MPa |

Table 2 The data used for calculation of the peak temperature at different weld pitch values for various aluminum alloys.

| Material | Solidus temperature, T_s , K | Thermal conductivity, k , $W m^{-1} K^{-1}$ | Specific heat, C_p , $J kg^{-1} K^{-1}$ | Shoulder radius, m | Pin radius, m | σ_8 , MPa | F |
|----------|-----------------------------------|--------------------------------------------------|----------------------------------------------|-----------------------|------------------|---------------------|------|
| AA7075 | 749 | 130 | 1200 | 0.0125 | 0.006 | 26.88 | 0.95 |
| AA2024 | 775 | 110 | 1200 | 0.0125 | 0.006 | 19.27 | 0.95 |
| AA5083 | 852 | 109 | 1200 | 0.0125 | 0.006 | 16.70 | 0.95 |

Table 3 Compositions of FSW processed aluminum alloys (wt.%) and their hardness in as welded condition.

| Alloy | Si | Fe | Cu | Mn | Mg | Ti | Zn | Cr | TMAZ Hardness (HV) | Ref. |
|------------|------|------|------|------|------|------|------|------|--------------------------|------|
| 6063-T5 | 0.48 | 0.2 | 0.02 | 0.03 | 0.52 | 0 | 0 | 0.01 | 40.0 | [67] |
| 6063-T5 | 0.48 | 0.2 | 0.02 | 0.03 | 0.52 | 0 | 0 | 0.01 | 44.0 | [67] |
| 6063-T5 | 0.44 | 0.18 | 0.01 | 0.04 | 0.48 | 0 | 0 | 0.01 | 48.0 | [68] |
| 7050-T7451 | 0.1 | 0.1 | 2.23 | 0 | 2.25 | 0 | 6.2 | 0 | 108.0 | [69] |
| 7050-T7451 | 0.1 | 0.1 | 2.23 | 0 | 2.25 | 0 | 6.2 | 0 | 109.9 | [69] |
| 7050-T7451 | 0.1 | 0.1 | 2.23 | 0 | 2.25 | 0 | 6.2 | 0 | 116.8 | [69] |
| 7050-T7451 | 0.1 | 0.1 | 2.23 | 0 | 2.25 | 0 | 6.2 | 0 | 121.1 | [69] |
| 7050-T7451 | 0.1 | 0.1 | 2.23 | 0 | 2.25 | 0 | 6.2 | 0 | 113.4 | [69] |
| 7050-T7451 | 0.1 | 0.1 | 2.23 | 0 | 2.25 | 0 | 6.2 | 0 | 116.4 | [69] |
| 7050-T7451 | 0.1 | 0.1 | 2.23 | 0 | 2.25 | 0 | 6.2 | 0 | 114.3 | [69] |
| 7050-T7451 | 0.1 | 0.1 | 2.23 | 0 | 2.25 | 0 | 6.2 | 0 | 117.2 | [69] |
| 7050-T7451 | 0.1 | 0.1 | 2.23 | 0 | 2.25 | 0 | 6.2 | 0 | 112.5 | [69] |
| 7050-T7451 | 0.1 | 0.1 | 2.23 | 0 | 2.25 | 0 | 6.2 | 0 | 115.4 | [69] |
| 7050-T7451 | 0.1 | 0.1 | 2.23 | 0 | 2.25 | 0 | 6.2 | 0 | 118.0 | [69] |
| 7050-T7451 | 0.1 | 0.1 | 2.23 | 0 | 2.25 | 0 | 6.2 | 0 | 124.1 | [70] |
| 2017-T351 | 0.52 | 0.29 | 4.29 | 0.5 | 0.6 | 0.02 | 0.08 | 0.02 | 125.0 | [71] |
| 2017-T351 | 0.52 | 0.29 | 4.29 | 0.5 | 0.6 | 0.02 | 0.08 | 0.02 | 140.0 | [71] |
| 2017-T351 | 0.52 | 0.29 | 4.29 | 0.5 | 0.6 | 0.02 | 0.08 | 0.02 | 133.0 | [71] |
| 5083-O | 0.14 | 0.2 | 0.01 | 0.65 | 4.62 | 0.1 | 0.01 | 0.01 | 105.0 | [72] |
| 5083-O | 0.14 | 0.2 | 0.01 | 0.65 | 4.62 | 0.1 | 0.01 | 0.01 | 116.0 | [72] |
| 5083-O | 0.14 | 0.2 | 0.01 | 0.65 | 4.62 | 0.1 | 0.01 | 0.01 | 130.0 | [72] |
| 1050-O | 0.1 | 0.29 | 0.01 | 0 | 0.02 | 0 | 0.01 | 0.02 | 32.0 | [72] |
| 1050-O | 0.1 | 0.29 | 0.01 | 0 | 0.02 | 0 | 0.01 | 0.02 | 44.0 | [72] |
| AW-6082-T6 | 1 | 0.5 | 0.1 | 0.7 | 0.9 | 0.25 | 0.2 | 0.1 | 85.0 | [73] |
| 1080 | 0.1 | 0.41 | 0.02 | 0.01 | 0.02 | 0 | 0.04 | 0.02 | 28.0 | [74] |
| 5052 | 0.45 | 0.45 | 0.1 | 0.1 | 2.5 | 0.25 | 0.1 | 0 | 70.0 | [75] |
| 6063-T6 | 0.4 | 0.35 | 0.1 | 0.1 | 0.68 | 0.1 | 0.1 | 0.1 | 76.2 | [76] |

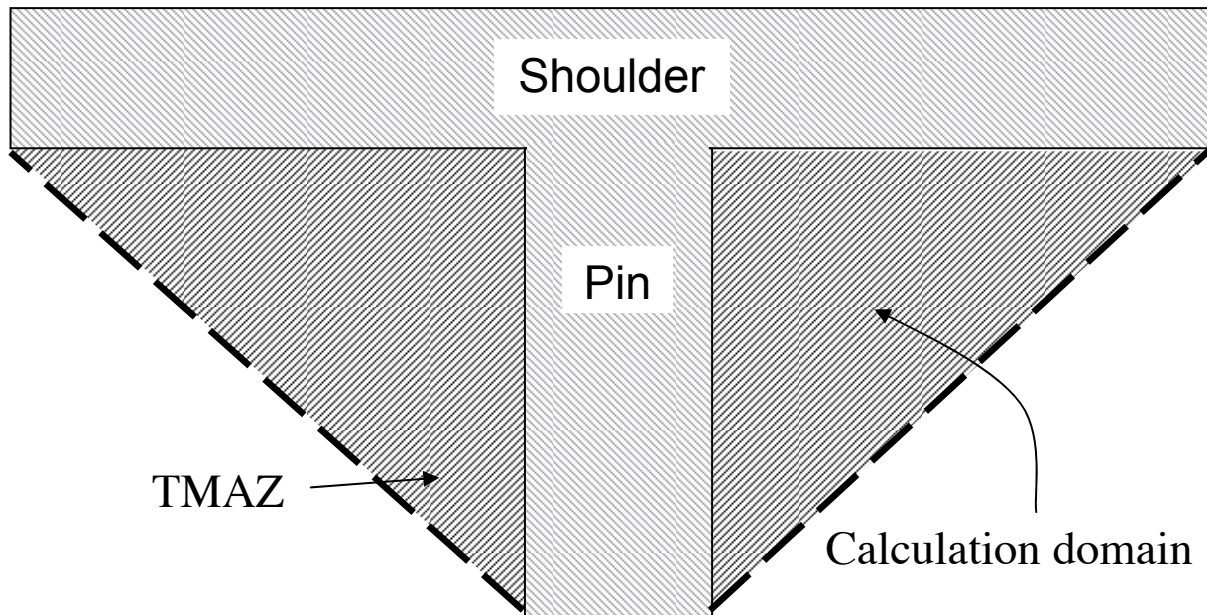


Fig. 1 Schematic diagram showing the domain for velocity field calculation. An approximate thermomechanically affected zone (TMAZ) geometry is shown by cross hatched region in the figure.

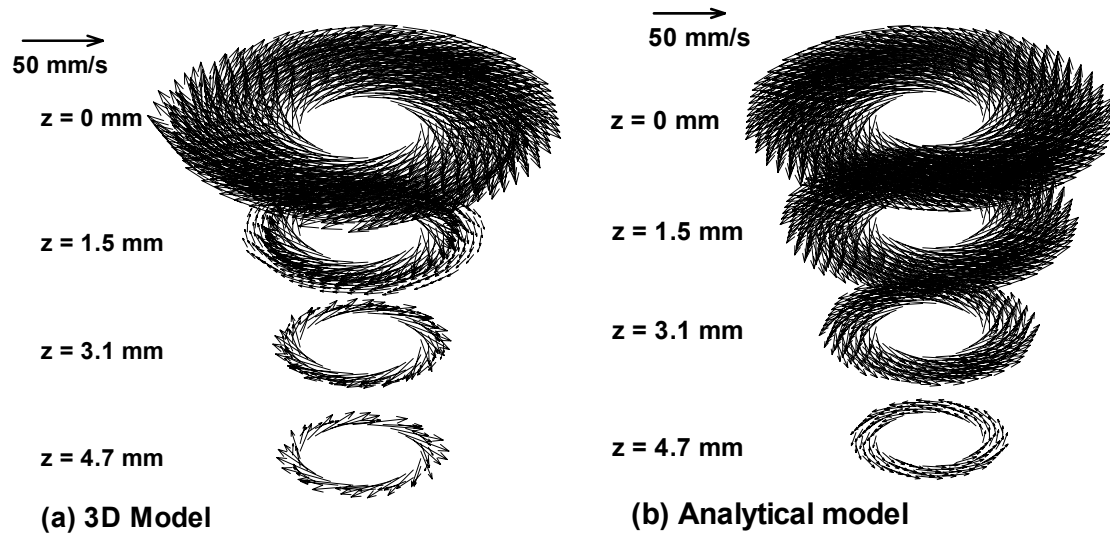


Fig. 2 The computed velocity fields in various horizontal planes for the FSW of AA2524. (a) results from a well tested numerical heat transfer and visco plastic flow code, and (b) from the proposed analytical solution.

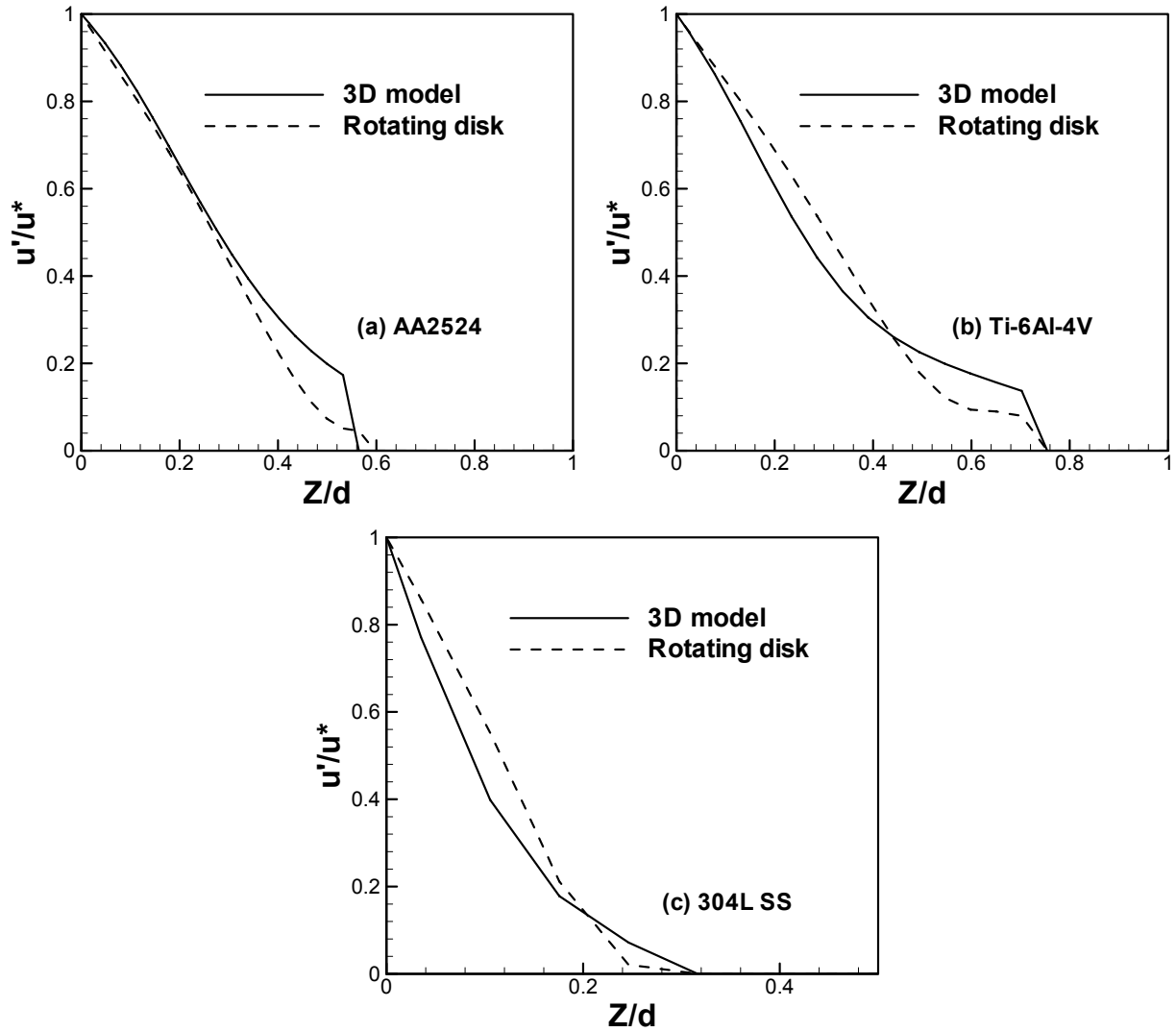


Fig. 3 The analytically computed velocities relative to the maximum velocity as a function of the dimensionless distance from the tool shoulder. (a) AA2524 (b) Ti-6Al-4V, (c) 304L SS. u' is the square root of sum of the three velocity components squared and u^* is the maximum velocity.

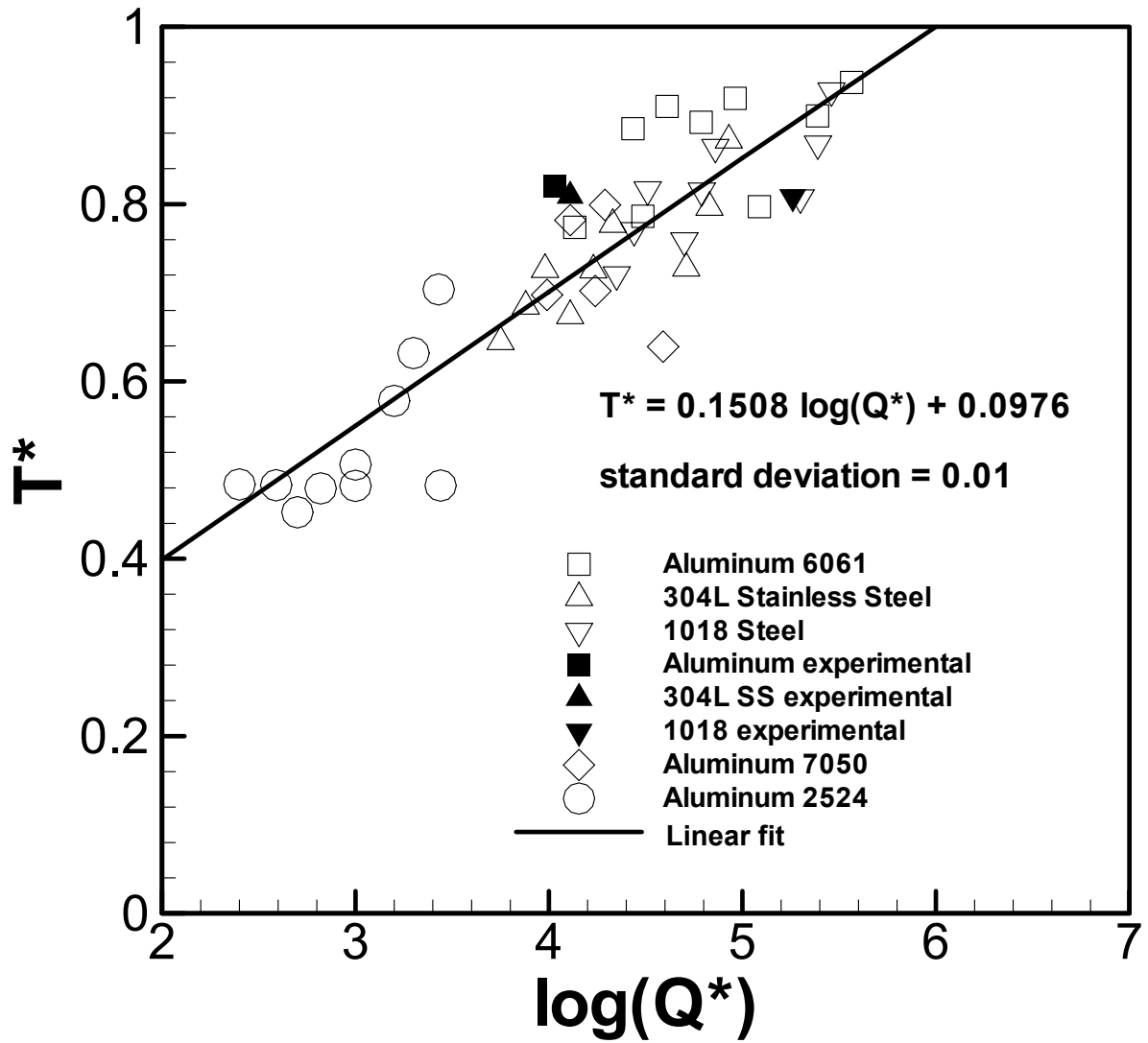


Fig. 4 Linear relationship between dimensionless temperature and log of dimensionless heat input.

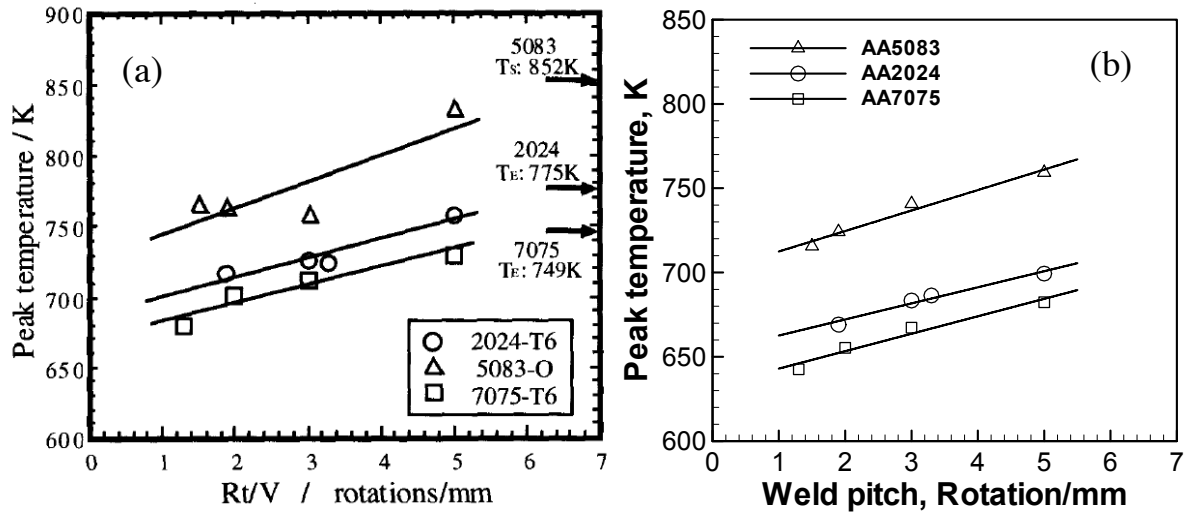


Fig. 5 Peak temperature against weld pitch for friction stir welding of various aluminum alloys. (a) Experimentally measured peak temperature [66] (b) Peak temperature from the proposed correlation.

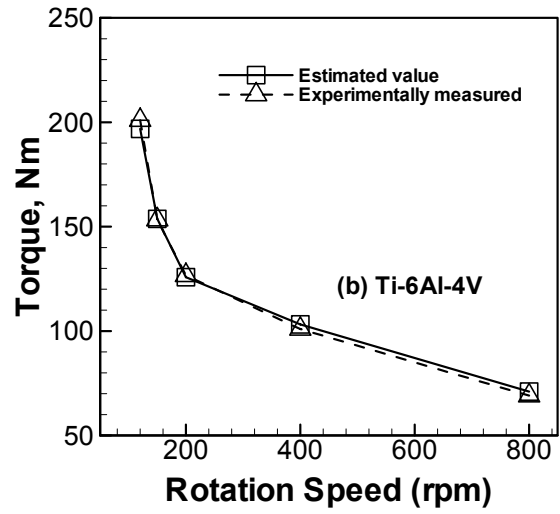
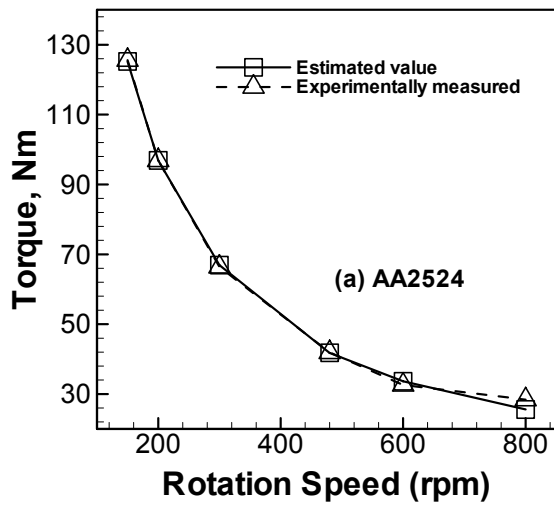


Fig. 6 Estimated and experimental torque values for FSW of (a) AA2524 and (b) Ti-6Al-4V alloy. The data used for the calculations are available in table 1.

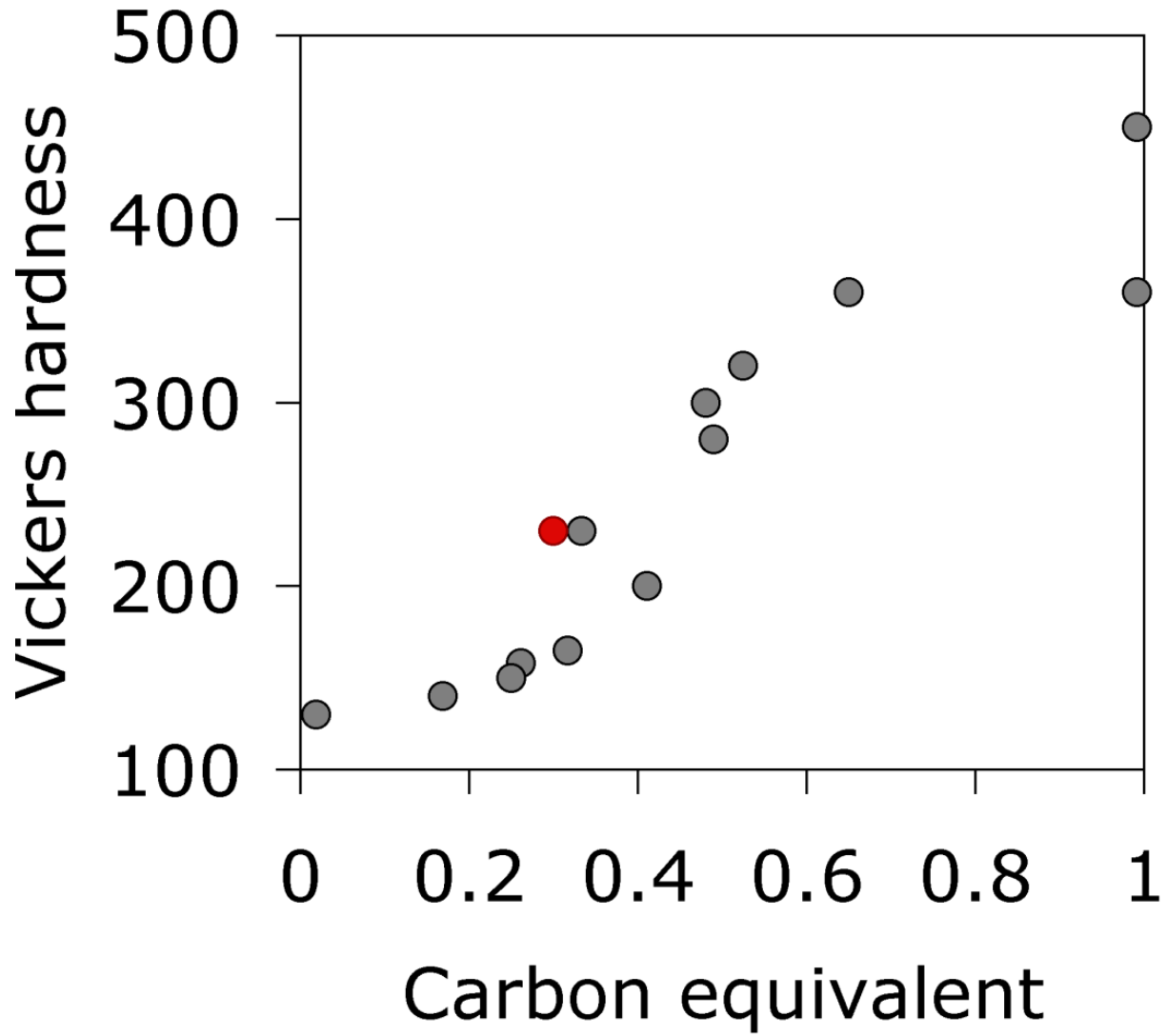


Fig. 7 The Vickers hardness of the TMAZ as a function of the IIW carbon equivalent of the steel. [61]

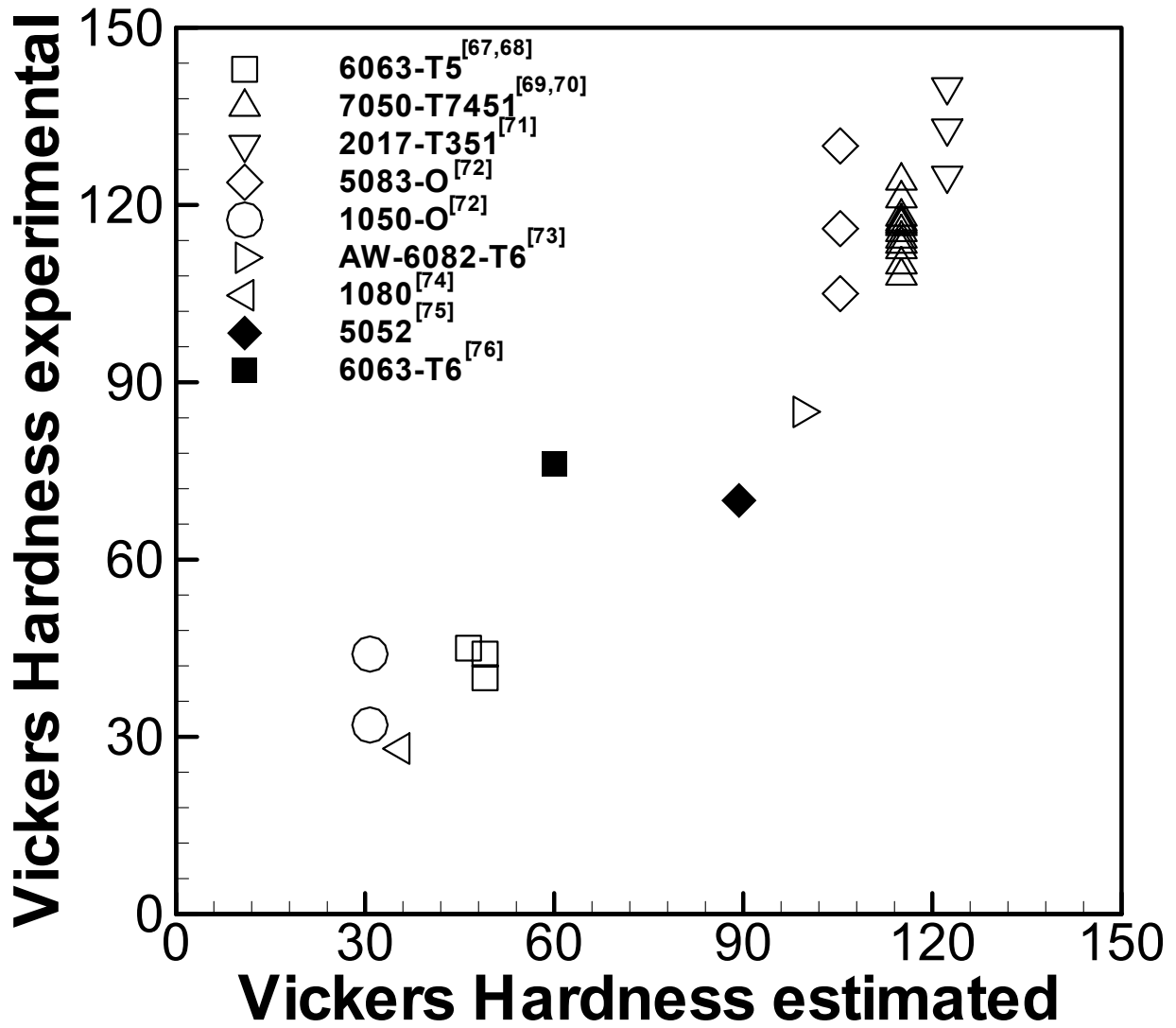


Fig. 8 A comparison of the experimentally measured Vickers hardness of TMAZ during FSW of various aluminum alloys with that estimated from alloy composition. [67-76]